Phase shift on reflection from metallodielectric photonic bandgap materials

M. Golosovsky,* Y. Neve-Oz, and D. Davidov
The Racah Institute of Physics, The Hebrew University of Jerusalem, Jerusalem 91904, Israel

A. Frenkel
ANAFA – Electromagnetic Solutions Ltd., P.O. Box 5301, Kiriat Bialik 27000, Israel
(Received 23 March 2004; revised manuscript received 14 June 2004; published 16 September 2004)

This paper reports phase-sensitive studies of the mm-wave reflection from a photonic crystal built from conducting spheres. We compare phase shift upon reflection from external interface to the phase shift on reflection from internal interface, the latter was estimated from the spectrum of Fabry-Perot resonances with photonic crystal mirrors. We show that the frequency-dependent phase shift upon internal reflection is consistent with the phase shift on external reflection from the whole crystal. We develop the analytical model that relates reflectivity of multilayers to admittances and to refractive indices of sublayers and takes account of magnetic permeability. This model yields a simple graphical procedure to determine the resonant frequencies of a Fabry-Perot resonator with photonic crystal mirrors. The model describes our results and results of two other groups fairly well.

DOI: 10.1103/PhysRevB.70.115105 PACS number(s): 42.70.Qs, 41.20.Jb

I. INTRODUCTION

Photonic crystals draw much interest today in view of potential applications in optical, microwave and infrared ranges. While their basic properties, such as transmission, dispersion relations, gap width, properties of defects, etc., have been extensively studied and are well understood now,[1] their phase properties, especially the frequency-dependent reflectivity phase shift, are not characterized enough. Experimental studies of the reflectivity phase shift using Fabry-Perot resonators with photonic crystal mirrors,[2,3] proved that the phase shift upon internal reflection is equal to the phase shift upon external reflection. While reflectivity phase is certainly important for the spectrum of Fabry-Perot resonators,[2,3] and for the phase modulators,[4] it acquires even more importance in connection with the Goos-Hanchen shift,[5] namely, the lateral displacement of a narrow beam upon reflection from the material which supports only evanescent waves. This effect arises from the dependence of the reflectivity phase on the wave vector orientation (which is a different guise for the frequency-dependent reflectivity phase). The Goos-Hanchen shift is well known in the context of total internal reflection, and was also observed in x-ray reflection from atomic planes.[6] Recently it has been predicted theoretically for photonic crystals[7,8] where it can serve as a basis for many interesting applications.

In this study we systematically explore the phase shift upon reflection from photonic crystal. We use a metallodielectric sample based on the array of conducting spheres[9–13] which has a wide photonic band gap and negligible absorption. We compare our experimental results to numerical simulations. Although we perform our experimental studies in the mm-wave range, our conclusions are quite general and applicable to optical wavelengths.

We also compare our results to the analytical model. To understand the physical origin of the frequency-dependent reflectivity phase in photonic crystals, it is natural to rely on the optics of multilayers. Optical reflectivity of multilayers was studied in the context of Fabry-Perot filters and dielectric mirrors.[5,14–16] Analytic expressions for the frequency-dependent phase shift upon reflection from the quarter-wavelength dielectric mirror were obtained by Babic and Corzine[17] using the coupled-mode model and assuming small contrast difference between the constituents. Later on, Brovelli and Keller,[18] using hyperbolic tangent substitution and transfer matrix method, extended this analysis to arbitrary contrast. Quite recently Garmire[19] analyzed finite length multilayers, while Abeles[14,15] took into account material dispersion. In all these works, the reflectivity phase is expressed through refraction indices of sublayers. However, it is well known that the optical properties of materials are determined by the refraction index $n=(\mu\epsilon)^{1/2}$ and admittance $Y=(\epsilon/\mu)^{1/2}$ as well.[20] Here μ is the magnetic permeability and ϵ is the dielectric permittivity. In optics $\mu=1$, hence $Y=n$, and all properties of multilayers may be recast through refraction indices. This is not necessarily true for photonic band gap materials where magnetic permeability plays an important role.[20,21,23–27] In particular, metallodielectric photonic crystal has an effective magnetic permeability which arises from the skin effect in the metallic consituent.[28–30] Even all-dielectric photonic crystal may have magnetic permeability $\mu\neq 1$ when considered as an effective medium.[21] Therefore the previous analysis of the reflectivity of multilayers should be revisited in order to take into account magnetic effects. We develop here a simple analytical derivation of the reflectivity of multilayers, based on transmission line analogy and the Bragg reflector model,[5] where we carefully distinguish between admittances and refraction indices. The resulting expressions are valid for $\mu\neq 1$. We successfully apply this model to describe our experimental data and the data of two other groups.[2,3] Our derivation is intended to serve as an auxiliary tool for the calculation of the photonic crystal reflectivity, while the rigorous calculation is best done using transfer matrix formalism.[22,23,31]

II. THE MODEL

A. Phase shift upon reflection from multilayer

We assume a periodic two-component multilayer $[AB]^N$ consisting of uniform sublayers A and B with thicknesses d_A, d_B, refraction indices n_A, n_B, and admittances Y_A, Y_B ($Y_A \neq Y_B$), related to the dielectric constant ϵ and the magnetic permeability μ of individual sublayers as follows: $Y=(\epsilon/\mu)^{1/2}$, $n=(\epsilon\mu)^{1/2}$ (in the visible range $Y=n$). Reflectivity of this multilayer is

$$R = \frac{Y_0 - Y_N}{Y_0 + Y_N}, \tag{1}$$

where Y_N is the effective admittance of the multilayer consisting of N unit cells and $Y_0=(377\Omega)^{-1}$ is the admittance of free space. In what follows, we divide all admittances by Y_0. The multilayer exhibits a stopband. For the frequencies inside the stopband the wave is evanescent, so the admittance is purely imaginary and for $N \gg 1$ it achieves a constant value, $Y_N \to Y_{\text{inf}}=js$. For such "infinite" multilayer, the reflectivity in the stopband is $R=e^{-j\Phi}$ where

$$\Phi = 2 \arctan s. \tag{2}$$

We calculate the admittance of the finite size $[AB]^N$ multilayer using recurrent procedure. Indeed, if we add to the front side of this multilayer an additional B sublayer, the admittance of the resulting $B[AB]^N$ multilayer is found using admittance transformation,

$$Y' = Y_B \frac{Y_N + jY_B \tan k_B d_B}{jY_N \tan k_B d_B + Y_B}, \tag{3}$$

where $k_B=2\pi f n_B/c$ is the wave vector. If we add to the front side of the resulting multilayer an additional A sublayer, the admittance of the resulting $[AB]^{N+1}$ multilayer is

$$Y_{N+1} = Y_A \frac{Y' + jY_A \tan k_A d_A}{jY' \tan k_A d_A + Y_A}. \tag{4}$$

However, for the frequencies inside the stopband and for $N \gg 1$, $Y_N \approx Y_{N+1} \approx Y_{\text{inf}}$. Then Eqs. (3) and (4) yield

$$s^2 + s\frac{(Y_B^2 - Y_A^2)\tan k_B d_B \tan k_A d_A}{Y_A \tan k_B d_B + Y_B \tan k_A d_A} + Y_A Y_B \frac{Y_A \tan k_A d_A + Y_B \tan k_B d_B}{Y_A \tan k_B d_B + Y_B \tan k_A d_A} = 0. \tag{5}$$

For the frequencies inside the gap, s is real, hence the determinant of Eq. (5) should be positive. This requirement yields the dispersion relation and defines the upper f_u and lower f_l stopband frequencies, while the solutions of Eq. (5) yield the phase of the reflectivity through Eq. (2). To avoid cumbersome algebraic expressions, we restrict ourselves to a particular case of the quarter-wavelength stack, i.e., $n_A d_A = n_B d_B$. Then Eq. (5) reduces to

$$s^2 + s(Y_B - Y_A)\tan\frac{\pi f}{2f_0} + Y_A Y_B = 0, \tag{6}$$

where

$$f_0 = \frac{c}{2(n_A d_A + n_B d_B)} = \frac{c}{2dn_{\text{eff}}} \tag{7}$$

is the midgap frequency, c is the speed of light, $d=d_A+d_B$ is the unit cell period, and n_{eff} is the effective refraction index of the crystal as a whole. The width of the gap is

$$\Delta f = f_u - f_l = \frac{4f_0}{\pi} \sin^{-1} \left| \frac{Y_A - Y_B}{Y_A + Y_B} \right|. \tag{8}$$

The solutions of Eq. (6) are

$$s^{HL} = \frac{(Y_A - Y_B)\tan\frac{\pi f}{2f_0}}{2} \left[1 + \left(1 - \frac{4Y_A Y_B}{(Y_A - Y_B)^2 \tan^2\frac{\pi f}{2f_0}} \right)^{1/2} \right] \tag{9}$$

for $Y_A > Y_B$ (high-low sequence) and

$$s^{LH} = \frac{(Y_A - Y_B)\tan\frac{\pi f}{2f_0}}{2} \left[1 - \left(1 - \frac{4Y_A Y_B}{(Y_A - Y_B)^2 \tan^2\frac{\pi f}{2f_0}} \right)^{1/2} \right] \tag{10}$$

for $Y_A < Y_B$ (low-high sequence). The identification of the solutions was made through comparison of Eqs. (9) and (10) to the limiting case of the admittance of the quarter-wavelength stack at midgap frequency, $Y_N=(Y_A/Y_B)^{2N}$ (which can be found by applying $2N$ times the well-known expression for the admittance of the quarter-wave plate), in such a way that $Y_N \to \infty$ for $Y_A > Y_B$, and $Y_N \to 0$ for $Y_A < Y_B$.

In the vicinity of the midgap frequency the Eqs. (2), (9), and (10) may be linearized. To this end we replace $\tan(\pi f/2f_0)$ by $2f_0/\pi(f_0-f)$ and substitute Eqs. (9) and (10) into Eq. (2). The resulting phase shift on reflection is

$$\Phi^{HL} \approx \pi + \frac{\pi(f - f_0)}{f_0(Y_A - Y_B)}, \tag{11}$$

$$\Phi^{LH} \approx \frac{\pi(f - f_0)}{f_0(Z_A - Z_B)}, \tag{12}$$

where $Z=Y^{-1}$ is the impedance (dimensionless). Note that at the midgap frequency, $\Phi^{HL}(f_0)=\pi$ and $\Phi^{LH}(f_0)=0$. The linear expansion given by Eqs. (11) and (12) holds for $|\Phi(f)-\Phi(f_0)| < (\pi/4)$.[19] If we replace Y by n, i.e., assume $\mu=1$, Eqs. (11) and (12) reduce to previous results.[15,17–19]

The linear frequency dependence of the phase can be interpreted as a virtual reflection from the plane shifted from the outer interface by $L_{ph}=\frac{1}{2}(\partial\Phi/\partial k)$. This phase penetration length[17] is calculated from Eqs. (11) and (12),

$$L_{ph}^{HL} = \frac{c}{4f_0(Y_A - Y_B)}, \tag{13}$$

$$L_{ph}^{LH} = \frac{cY_AY_B}{4f_0(Y_B - Y_A)} = \frac{c}{4f_0(Z_A - Z_B)}. \quad (14)$$

Note that in both cases L_{ph} is positive, i.e., reflection effectively occurs *inside* the crystal. With respect to pulse reflection this means *positive* group delay.

B. Fabry-Perot resonances

The spectrum of a Fabry-Perot resonator with dielectric mirrors is determined by the frequency-dependent reflectivity phase. To model it, we assume that our multilayer $[AB]^N$ is split in two halves with a separation L between them. The space between the halves operates as a Fabry-Perot resonator. We assume that only a single plane wave (i.e., zero-order Floquet mode) could propagate in the resonator space. Transmission through the two halves of the photonic crystal coupled through the Fabry-Perot resonator is given by

$$T_{FP} = \frac{e^{i(2\pi fL/c)}S_{12}^2}{e^{i(4\pi fL/c)} - S_{11}^2}, \quad (15)$$

where S_{12} and S_{11} are complex transmission and the reflection coefficients for each of the halves. For sufficiently large number of layers, $N \gg 1$, and for the frequencies in the stopband, $S_{12} \ll 1$ and $S_{11} \approx e^{-j\Phi}$, where Φ is the phase shift upon reflection from the infinite crystal. Then Eq. (15) yields resonant frequencies f,

$$\frac{4\pi Lf}{c} + \Phi_1(f) + \Phi_2(f) = 2m\pi, \quad (16)$$

where Φ_1, Φ_2 are the phase shifts upon reflection from each half of the multilayer. If one half of the multilayer is $[AB]^{N/2}$, another half is $[BA]^{N/2}$. In other words, if the front layer in one half is A, the front layer in another half is B (Fig. 5). Therefore, if Φ_1 is given by Eq. (11), then Φ_2 is given by Eq. (12) (with the indices A and B interchanged). The sum of these two phase shifts is found from Eqs. (2), (9), and (10),

$$\begin{aligned}\Phi_1 + \Phi_2 &= 2\ \arctan(s^{HL} - s^{LH}) \\ &= 2\ \arctan\left[\frac{|Y_A - Y_B|}{1 + Y_AY_B}\right. \\ &\quad \left.\times\left(1 - \frac{4Y_AY_B}{(Y_A - Y_B)^2\ \tan^2\dfrac{\pi f}{2f_0}}\right)^{1/2}\tan\frac{\pi f}{2f_0}\right]. \quad (17)\end{aligned}$$

Since at the gap edges $s^{HL} = s^{LH}$, then $\Phi_1 + \Phi_2$ is equal to zero at the lower edge, is equal to π at the midgap and to 2π at the upper edge.

To find the resonant frequency corresponding to a certain L, we substitute Eq. (17) into Eq. (16) and solve for $f(L)$. For any given m and L there is only one solution, provided $Y_A, Y_B \geq 1$. In the vicinity of the midgap the solution can be found quite easily. We substitute the linear expansion of Eq. (17),

$$\Phi_1 + \Phi_2 \approx \pi + \frac{\pi(f - f_0)(1 + Y_AY_B)}{f_0|Y_A - Y_B|} \quad (18)$$

into Eq. (16), recast it through the wavelength and find linear dependence of the resonant wavelength λ_{FP} on L,

$$\lambda_{FP} = \lambda_0\frac{L + L_{ph1} + L_{ph2}}{\left(\dfrac{m}{2} - \dfrac{1}{4}\right)\lambda_0 + L_{ph1} + L_{ph2}}. \quad (19)$$

Here, $\lambda_0 = c/f_0$ is the midgap wavelength, and L_{ph1}, L_{ph2} are the phase penetration depths into each half of the multilayer, which are given by Eqs. (13) and (14). Equation (19) predicts that $\lambda_{FP}(L)$ consists of a series of straight lines intercepting at the horizontal axis; the intercept is the sum of the phase penetration depths, $L_{ph1} + L_{ph2}$. Each line corresponds to a certain m in Eq. (16). Note, that for $L = p\lambda_0/4$, where $p = 1, 3, 5\ldots$, the resonance wavelength is exactly at the midgap, i.e., $\lambda_{FP} = \lambda_0$, while for $L \to 0$ the resonance wavelength is at the stopband edges. This allows us to estimate the resonance wavelengths using graphical procedure illustrated in Fig. 5. Indeed, assuming that the admittance of the low-index material is close to unity, i.e., $Y_B \simeq 1$, then Eq. (19) may be recast through experimentally measured parameters such as midgap wavelength f_0 and gap width Δf,

$$\frac{\lambda_{FP}}{\lambda_0} \approx \frac{\dfrac{L}{\lambda_0} + \dfrac{f_0}{\pi\Delta f}}{\dfrac{m}{2} - \dfrac{1}{4} + \dfrac{f_0}{\pi\Delta f}}. \quad (20)$$

Here we used Eqs. (7) and (8). In this case the horizontal intercept in Fig. 5 is determined by the experimentally measured parameters, i.e., $L_{ph1} + L_{ph2} \approx (f_0/\pi\Delta f)$. Of course, Eqs. (19) and (20) are valid only in the vicinity of the midgap, while at the gap edges one should use Eqs. (16) and (17).

III. EXPERIMENTAL SETUP

Figure 1 shows the experimental setup. Our building block is an array of 230 steel spheres of 2 mm diameter placed on a 0.67 mm thick plexiglas plate. In this plate we drilled a hexagonal array of small holes 2.9 mm apart and mounted our spheres in the holes, in such a way that the spheres slightly protrude through the plate. In order to match the stopband to the frequency range of our source we removed 30% of the spheres. This results in "diluted" hexagonal lattice (the in-plane particle arrangement is shown in the inset in Fig. 1). The spheres can be considered as perfect conductors since for our frequency range, the skin depth is much smaller than radius. Moreover, since the sphere radius is such that $kr \lesssim 1$, all Mie resonances of the spheres[32] are above our experimental frequency range.

Ten layers of spheres were arranged in a stack (Fig. 1). The layer spacing of 4.3 mm was fixed by appropriate spacers. The layers were assembled in such a way that the spheres formed the columns across the stack. However, our experimental results turned out to be insensitive to small lateral shift of one layer relative to another. This is probably

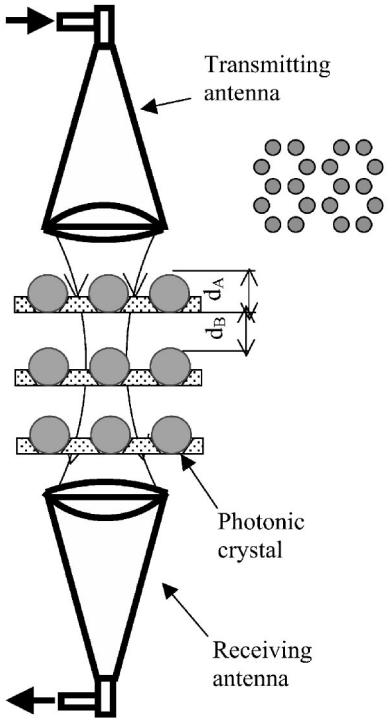

FIG. 1. Measurement setup. Standard gain microwave horns are connected to HP8510C Vector Network Analyzer and are terminated by two home-made collimating teflon lenses. The sample is a stack of 10 plexiglas plates, each of them containing 230 steel spheres of 2 mm diameter. The in-plane arrangement of the spheres is shown in the inset. The nearest-neighbor in-plane distance is 2.9 mm and the layer spacing is $d=4.3$ mm.

due to the fact that the interlayer separation is rather big, $d>r, d>\lambda/2\pi$, hence near fields of the scatterers in adjacent layers do not overlap.

Mm-wave transmission and reflection was measured in the frequency range of 20–50 GHz, using a HP8510C Vector Network Analyzer and two standard gain horn antennas equipped with collimating teflon lenses. The inner curvature of the lens is 15 cm, the outer curvature is 30 cm, the distance between antennas is 28 cm, the beamwidth is 6 cm. The sample is mounted symmetrically between antennas and its cross section slightly exceeds the beamwidth. To prevent edge effects we set two 6 cm diameter apertures above and below the sample. Calibration for the reflectivity measurements was performed using a thin aluminum foil covering the upper layer of the array. This should represent a perfect short.

IV. EXPERIMENTAL RESULTS AND COMPARISON TO THE MODEL

Figure 2 shows our experimental results. Transmission measurements clearly reveal a stopband at 25–39 GHz which becomes exponentially deeper upon increasing number of layers N (not shown here), i.e., transmittance $\sim \exp -(2Nd/l)$ where d is the unit cell period and l is the localization length (Bragg attenuation length). Localization length

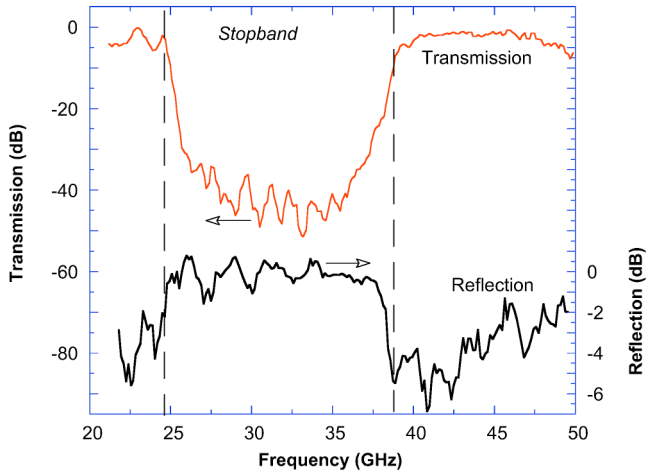

FIG. 2. Transmittivity and reflectivity of a 10-layer sample. We clearly see the stopband at 25–39 GHz. The reflectivity in the stopband is close to unity.

in the stopband is very short, $l=1.5d$, so this 10-layer stack can be considered as infinite one. In the frequency range corresponding to the stopband, the electromagnetic wave does not penetrate into the stack and is totally reflected, hence the reflectivity is close to unity (Fig. 2). The reflectivity phase is strongly frequency dependent (Fig. 3) and the phase shift at the midgap is close to π, as predicted by the model [Eq. (11)]. Similar results were obtained for the stack constructed from 3 mm diameter steel spheres (not shown here).

To achieve quantitative comparison to the model, we identify the constituents: the sublayer A consists of conducting spheres mounted in the plexiglas plate, while the sublayer B is the spacing between the layers of spheres, i.e., $d_A=2r=2$ mm; $d_B=2.3$ mm; $n_B=1$, $Y_B=1$. (We do not consider the plexiglas plate as a separate layer since its optical thickness does not exceed $\lambda/6$ so that the standing wave

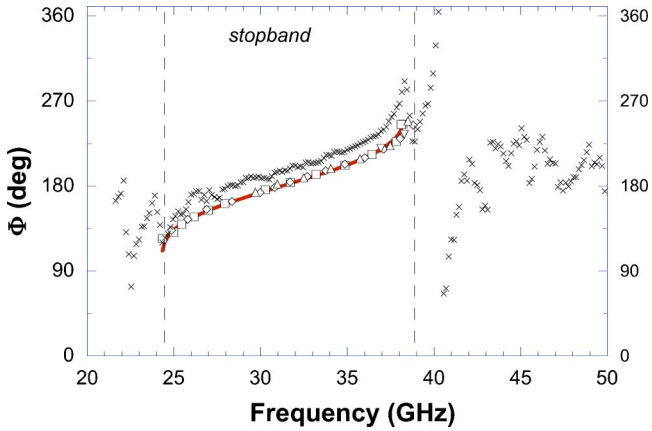

FIG. 3. The phase shift upon external reflection from the sample shown in Fig. 1. The crosses show experimental data for reflection from external interface, continuous solid line shows model prediction [Eq. (9)] and open symbols stand for the phase shift upon internal reflection from photonic crystal mirrors. The latter data were retrieved from the spectrum of defects (Fig. 6). Note quasilinear frequency dependence of the reflectivity phase in the stopband.

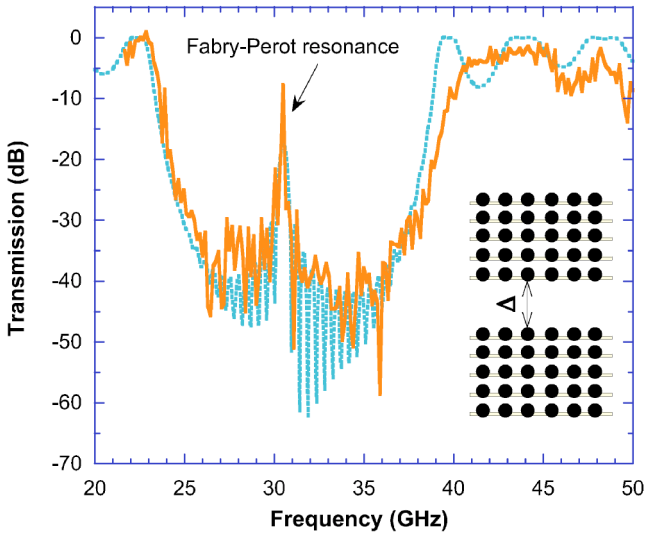

FIG. 4. Mm-wave transmission through the 10-layer stack which has been split on two halves, each containing five layers. The separation between the two halves is $\Delta=6$ mm. Note a sharp peak at 30 GHz. We ascribe this peak to a Fabry-Perot resonance between two halves of the structure operating as mirrors. The dashed line shows numerical simulation of the microwave transmission through this stack using CST/Microwave Studio software (Ref. 35).

resonances do not occur there in our frequency range.) The effective refraction index of the layer of conducting spheres, $n_A=1.19$, was found by substitution of the experimental value of the midgap frequency ($f_0=31.7$ GHz) into Eq. (7). Note that the condition of a quarter-wavelength stack is satisfied here pretty well, $n_A d_A/n_B d_B=1.03$; and at the center of the gap $k_A d_A=0.51\pi$, as expected. The effective admittance of the sublayer of conducting spheres embedded into plexiglas plate, $Y_A=2.04$, was found by substitution of the experimentally found stopband width $\Delta f=14.3$ GHz and midgap frequency $f_0=31.7$ GHz into Eq. (8). Note that $Y_A\neq n_A$, as expected for a metallodielectric composite where $\mu\neq 1$.[28–30,33] We calculate the reflectivity phase using Eqs. (2) and (9), since $Y_A>Y_B$. The calculated phase is shown as a continuous line in Fig. 3. Experimental points (crosses) demonstrate the same frequency dependence although they are shifted up by 15°. This discrepancy is attributed to the uncertainty in the position/flatness of the calibration plane in the external reflectivity measurements. (Note that 1 mm uncertainty in the position of the calibration plane results in 30° phase shift.)

To construct a Fabry-Perot resonator, we split this stack into two halves and displaced one of the halves in the direction perpendicular to the layers by L. The distance between the splitted layers is $\Delta=L+d_B$. This operation does not affect the width of the gap but results in one or a few sharp transmission peaks inside it (Fig. 4). These peaks appear not only when we set two halves of the sample further apart ($L>0$) but when we bring them closer as well ($L<0$). To analyze the spectrum of these peaks as suggested by the model (Fig. 5), we plot the resonant wavelength versus separation and find that experimental points are grouped in a few series (Fig. 6), whereby the wavelength in each series linearly depends on L. The resonant wavelength is equal to the midgap wavelength each time when L is an odd multiple of $\lambda_0/4$. All these linear dependences intersect in one point on the horizontal axis. The experimentally found horizontal intercept of 0.8 agrees with the value of 0.71 predicted by Eq. (20).

The same analysis is applied to the results of Beaky *et al.*[3] who studied the two-dimensional (2D) photonic crystal consisting of a square lattice of cylindrical alumina rods with a few missing rows. When we plot the spectrum of resonances in this system in the coordinates of wavelength-separation, we find that experimental points are grouped in a few series, whereby the wavelength in each series linearly depends on separation L (Fig. 7). The resonant wavelength passes through the midgap each time when L is an odd multiple of $\lambda_0/4$. All these linear dependences intersect at one point on the horizontal axis. To compare this horizontal intercept to model prediction, we model this 2D photonic crystal as a

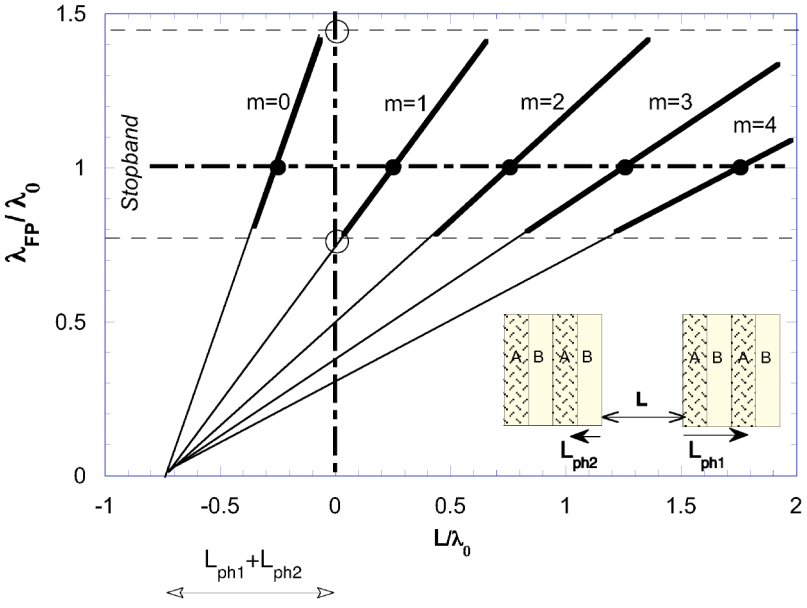

FIG. 5. Schematic representation of the spectrum of Fabry-Perot resonator with dielectric mirrors, as a function of the resonator length. Note straight lines with common intercept at the horizontal axis. The sections of these lines passing through the stopband (thick solid lines) define possible values of resonant wavelengths. When the resonator length is an odd multiple of $\lambda_0/4$, where λ_0 is the midgap wavelength, the resonance occurs at λ_0.

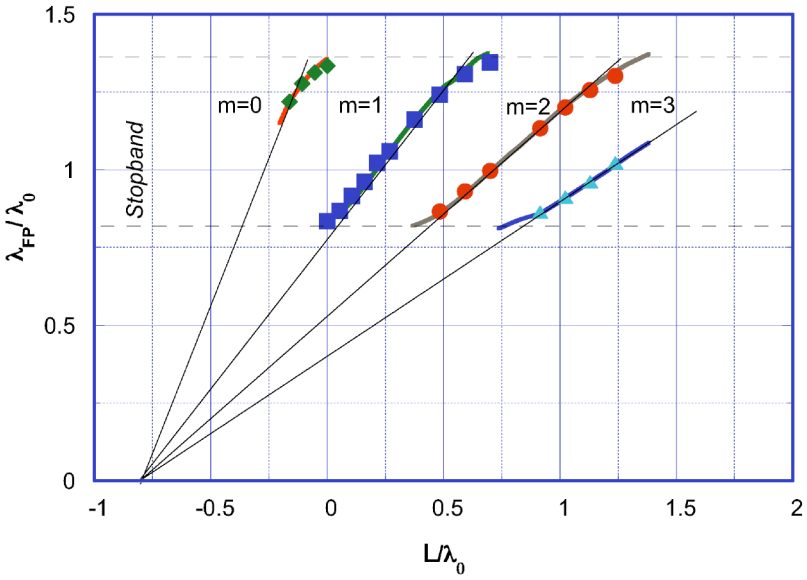

FIG. 6. The wavelength corresponding to transmission peaks shown in Fig. 4 as a function of the separation L between the two halves of the stack. $L=0$ corresponds to the regular sample shown in Fig. 1. The symbols show experimental results, thick solid lines show results of numerical simulations, thin solid lines show linear dependences predicted by Eq. (20).

two-layer system, where sublayer A is a row of dielectric rods and sublayer B is the air spacing between the rows of the rods. The sublayer thickness is $d_A=2r=6.35$ mm and $d_B=14.45$ mm. We substitute $n_B=1$, $Y_B=1$, $\Delta f=3$ GHz, $f_0=5.3$ GHz into Eqs. (7) and (8) and find $n_A=2.2$, $Y_A=2.7$. (Although here $Y_A \neq n_A$, while in all-dielectric composite we expect $Y_A=n_A$, we do not believe that this deviation indicates effective magnetic properties of this photonic crystal. We trace this deviation to the error of replacing a plane of scatterers by a uniform layer with sharp interfaces.) Here, the condition of a quarter-wavelength stack is also satisfied well, $n_A d_A/n_B d_B=0.94$; and at the center of the gap $k_A d_A=0.49\pi$, as expected. The horizontal intercept of 0.7 found in the experiment is not far from the value 0.55 predicted by Eq. (20).

The spectrum of resonances in a woodpile array of dielectric rods measured by Ozbay and Temelkuran[2] can be accounted for along the similar lines. Here, $f_0=13$ GHz, $\Delta f=6$ GHz. Despite a considerable deviation from the quarter-wavelength condition ($n_A d_A/n_B d_B=1.58$), the model predicts the spectrum of resonances here pretty well. Indeed, we find that experimental points are grouped in two series, whereby the wavelengths in each series linearly depend on separation (Fig. 8). The horizontal intercept of 1 that we find in the experiment is not far from the value 0.7 predicted by Eq. (20).

We conclude that for these three different materials (conducting spheres, dielectric rods, woodpile structure), our model describes fairly well the spectrum of Fabry-Perot resonances with photonic crystal mirrors and relates it to the frequency-dependent reflectivity phase.

Now we go back to our sample and compare the phase shift on external reflection to the phase shift on internal reflection derived from Fabry-Perot resonances. Here we use the fact that in our sample the sublayer B is the air, hence the effective length of the resonator may be also written as $\Delta=L+d_B$, in such a way, $\Phi_2=\Phi_1-(4\pi L f/c)$. To determine Φ_1 we use the procedure first proposed by Ref. 2. We plot

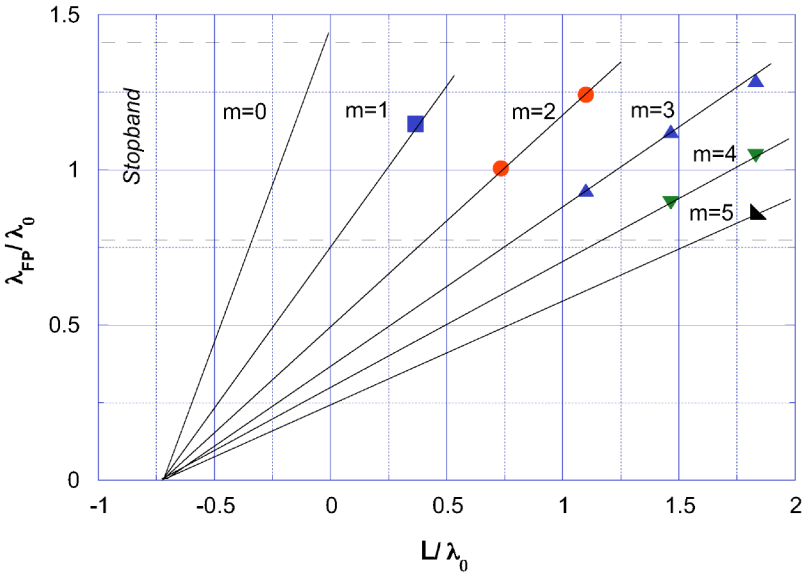

FIG. 7. The resonant wavelength in a 2D array of dielectric rods (Ref. 3) split in two parts, as a function of separation L between the two halves of the stack. $L=0$ corresponds to the ideal crystal. The symbols show experimental results, thin solid lines show linear dependences predicted by Eq. (20).

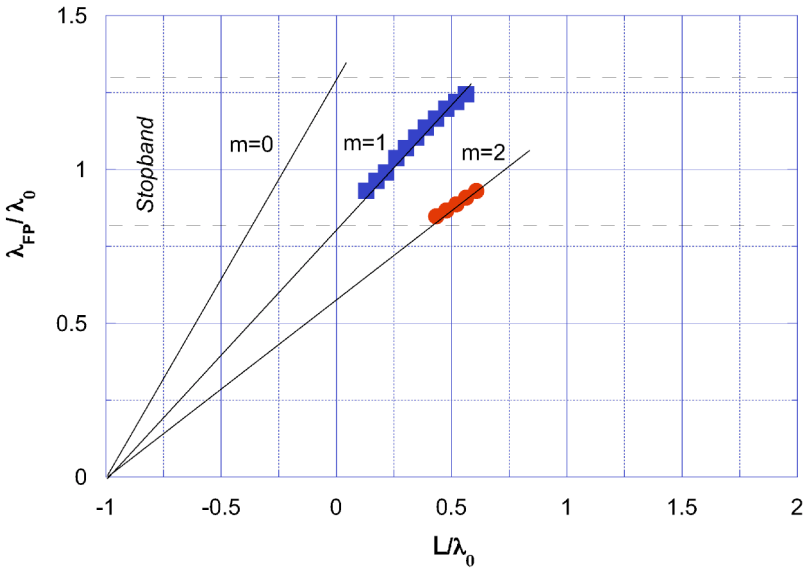

FIG. 8. The resonant wavelength corresponding to transmission peaks in the 3D woodpile array of dielectric rods (Ref. 2) split in two parts, as a function of separation L between the two halves of the stack. $L=0$ corresponds to the ideal crystal. The symbols show experimental results, thin solid lines show linear dependences predicted by Eq. (20).

experimentally found values of $2\pi\Delta f_{FP}(\Delta)/c$ versus resonant frequency, f_{FP}. This results in several series of experimental points displaced by π, each series corresponding to a particular m in Eq. (16). We identify mode numbers m, subtract multiples of π and obtain a single-valued dependence $\Phi(f)$ which is shown by open symbols in Fig. 3. At the next step we compare the phase shift on internal reflection to the phase shift on external reflection from the perfect crystal (Fig. 3, crosses). Note that both phase shifts are almost identical inside the gap. This is quite trivial for $\Delta \gg d$, where d is the unit cell period. However, it is surprising that the coincidence persists for $\Delta \sim d$ where strong near-field effects are expected; and even more surprising that it persists for $\Delta < d$ where *a priori* we hardly expect any resonances at all. (Indeed, if the reflection were occurring at the interface between photonic crystal and air, the first standing wave resonance in the splitted photonic crystal corresponds to condition $\Delta = \lambda/2$. For $\Delta < d$ the resonant wavelength is beyond the gap.)

V. COMPUTER SIMULATIONS

The simplifying assumption of a single plane wave within the Fabry-Perot resonator space [see Eqs. (15) and (16)], calls for accurate numerical simulations, especially at small separations.

We first studied a model of a Fabry-Perot resonator with infinite lateral extent. Due to the 2D periodicity of the photonic crystal, we can accurately model the infinite structure by a single unit cell with periodic boundaries. To this end we used Ansoft/HFSS,[34] a commercial finite element solver for Maxwell equations that has the capability of imposing periodic boundary conditions. The numerical model has five layers of metallic spheres for both reflectors, and includes also the plexiglas plates that hold the spheres in place. The hexagonal lattice is replaced by an equivalent square lattice with exactly the same photonic band gap. S parameters for both the whole Fabry-Perot resonator and the single reflector were calculated over a broad band of frequencies. We then compare the predictions of Eq. (15)—as derived from the FEM simulation of a single five-layers reflector—with the numerical FEM simulation of the complete resonator (two five-layers reflectors), and an excellent agreement is observed (Fig. 9). We find that the near-field effects of the evanescent waves are properly accounted for by the S parameters of the single reflector, so that the assumption of a single plane wave within the Fabry-Perot resonator is fully justified.

We then proceeded to simulate the finite-size resonator. Due to the large size (relative to wavelength) of the resonator we used CST/Microwave Studio,[35] a commercial FDTD solver that is more efficient in terms of computational resources. The complete finite-size resonator with the hexagonal lattice is analyzed. Figure 4 shows our experimental re-

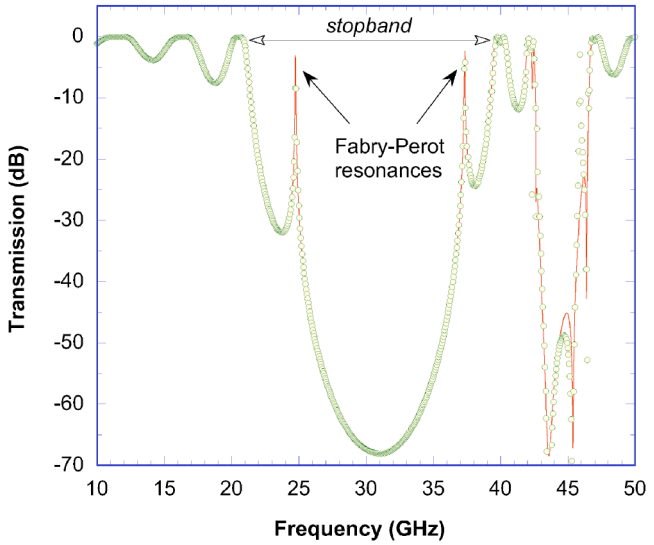

FIG. 9. Numerical simulation of the microwave transmission through the 10-layer stack shown in Fig. 4, using ANSOFT software (Ref. 34). The symbols show numerical simulation assuming infinite lateral extent of the stack. Solid line shows prediction of Eq. (15) assuming Fabry-Perot resonator with photonic crystal mirrors consisting of five bilayers each. The separation between the halves is $L=4.5$ mm ($L/\lambda_0=0.32$).

sults and the full-wave FDTD simulations, and a very good correspondence is observed. The low-level ripple of the simulated results originates from the finite sampling in time and the FFT transformation used to transform the time-domain results into frequency-domain results.

VI. DISCUSSION

A. Applicability of the Bragg reflector model

We have shown that the phase shift on reflection from several different photonic crystals can be estimated using a Bragg reflector model which takes into account magnetic effects. This model was developed to account for the optical properties of continuous multilayers. To account for photonic crystals, they should be represented as a sequence of layers where each layer is characterized by some effective dielectric constant and magnetic permeability. This requires some kind of effective-medium approximation[21,36–38] *for each layer*. The limits of such effective-medium approach to photonic crystals, which in fact are ordered arrays of scatterers, were analyzed by Lalanne[38] who showed that it works well only when the scatterers can be considered as dipoles.[29,39] It is well known that the dipole approximation is good for the scatterers of arbitrary shape, provided $kr<1$, where r is the size of the scatterer and k is the wave vector. Since in our experimental conditions $kr \lesssim 1$, the success of the combination of the Bragg reflector model and effective-medium approximation is not surprising. This can be formulated differently. To approximate a planar array of scatterers by a uniform layer, the near fields of the adjacent layers should not overlap. This is justified for small scatterers, whose near field consists of quickly decaying evanescent waves;[40] while it may be problematic for the scatterers with the size comparable to wavelength since they give rise to propagating waves.

In other words, for clearly defined layered structures, the Bragg reflector approximation is a useful tool to estimate localization length, position, and width of the gap.[13] Of course, not every 3D dielectric photonic band-gap crystal can be approximated by a multilayer, because sometimes the layers with distinctly different electrical properties cannot be clearly identified. Typical examples would be the original diamond lattice[41,42] and woodpile structures.[2,31,38] However, our results for the phase shift upon reflection may, nevertheless, be valid for these and other materials as well. To support this conjecture we recast Eqs. (12) and (11) using Eq. (8) and find

$$\Phi^{HL} \approx \pi + \frac{2(f-f_0)}{Y_{\text{ave}}\Delta f}, \tag{21}$$

$$\Phi^{LH} \approx \frac{2(f-f_0)}{Z_{\text{ave}}\Delta f}. \tag{22}$$

Here $Y_{\text{ave}}=(Y_A+Y_B)/2$ and $Z_{\text{ave}}=(Z_A+Z_B)/2$ is the average admittance (impedance) of the medium. Since these equations do not depend explicitly on the properties of the individual layers, they may be valid for any material exhibiting stopband, such as a uniform material with strong dispersion resulting in a negative dielectric constant or negative magnetic permeability, or a random media demonstrating localization.[45]

B. Comparison to the uniform medium

In the following step we compare reflectivity of a photonic crystal in the frequency range corresponding to the gap, to the reflectivity of an infinitely long uniform medium which supports only evanescent waves (for example, a dielectric under conditions of total internal reflection), e^{-qz}, where q^{-1} is the attenuation length. The admittance of such medium is $Y=-jq/\mu\omega$, hence the phase shift on reflection is $\Phi=\pi+2\arctan(\mu k/q)$, where μ is the magnetic permeability and k is the wave vector in free space. Following Ref. 17, we compare the phase penetration length, $L_{ph}=\frac{1}{2}(\partial\Phi/\partial k)$, to the energy penetration length, $L_E=1/2q$. Assuming frequency independent q and for $q \gg k$, we find $L_{ph} \simeq \mu/2q = \mu L_E$, hence in nonmagnetic media, $L_{ph}=L_E$.

In the context of photonic crystals this relation generally does not apply. Indeed, the energy penetration length into infinitely long photonic crystal is $L_E=L_B/2$, where $L_B=d/\ln(Y_A/Y_B)$ is the Bragg attenuation length[5] (localization length) which is very different from Eqs. (13) and (14). Only in the limit of small contrast, $\Delta Y=Y_A-Y_B \ll Y_A, Y_B$, when the Eqs. (7), (13), and (14) can be simplified and yield $L_{ph}^{HL} \approx nd/2\Delta Y$, $L_{ph}^{LH} \approx ndY^2/2\Delta Y$; there is some similarity to the uniform medium. Indeed, comparison to the energy penetration length, $L_E \approx dY/2\Delta Y$, yields $L_{ph}^{HL}=\mu_{\text{eff}}L_E$ and $L_{ph}^{LH}=\epsilon_{\text{eff}}L_E$, where $\epsilon_{\text{eff}}=nY$, $\mu_{\text{eff}}=n/Y$ are average dielectric permittivity and magnetic permeability of the whole crystal. Only for the case of HL sequence the relation between L_E and L_{ph} is the same as that for the uniform media, while for the LH sequence this relation is certainly different. (The LH sequence is known to have the unusual optical properties, in particular, anomalous dispersion.)[14] Hence, with respect to the phase properties, photonic crystal in general *cannot* be viewed as a uniform material with some effective parameters.

C. Magnetic effects in photonic crystals

These effects were usually mentioned only in connection to optical activity. Silverman and Sohn[43] demonstrated the importance of magnetic effects for the optical reflectivity of chiral media, while Pendry *et al.*[23] recently raised this question with respect to left-handed materials. While the meaning of the effective magnetic permeability for magnetic materials and composites built of magnetic constituents is more or less clear, the emergence of high-frequency magnetic permeability in the composites built of intrinsically nonmagnetic materials is controversial.[25] It is also known that in materials with high dielectric constant, the high-frequency dielectric relaxation may mimic magnetic permeability.[44] As suggested by O'Brien and Pendry,[20] instead of using effective ϵ and μ, the properties of photonic crystals can be better described using another pair of independent parameters, namely, effective refraction index n_{eff} and admittance Y_{eff}, which are less controversial. Indeed, the optical properties of multilayers

are conveniently described by the transfer matrix formalism[22] where wave propagation is represented by the product of phase matrices and reflectivity matrices. The phase matrix depends only on the thickness and refraction index n of the layer while the reflectivity matrix depends only on the reflectivity at the interfaces, i.e., on the admittance Y. Since n and Y are independent material parameters (in such a way that the relation $Y=n$ for nonmagnetic material is quite accidental), this approach treats magnetic and nonmagnetic materials on an equal basis.

VII. CONCLUSIONS

We achieved understanding of such important property of photonic crystals as the frequency-dependent reflectivity phase and provided analytical tools to deal with it. Our results can be used in applications, of which especially promising may be those based on the Goos-Hanchen shift. Since photonic crystals may be made tunable, we can envisage tunable resonators, phase modulators, or electronic beam steering upon reflection from the tunable photonic crystal.

ACKNOWLEDGMENTS

This work was supported by the VW Foundation, Israeli Science Foundation, and Israeli Ministry of Science and Technology.

*Electronic address: golos@vms.huji.ac.il

[1] J. D. Joannopoulos, R. D. Meade, and J. N. Winn, *Photonic Crystals Molding the Flow of Light* (Princeton University Press, New Jersey, 1995).
[2] E. Ozbay and T. Temelkuran, Appl. Phys. Lett. **69**, 743 (1996).
[3] M. M. Beaky, J. B. Burk, H. O. Everitt, M. A. Haider, and S. Venakides, IEEE Trans. Microwave Theory Tech. **47**, 2085 (1999).
[4] I. Abdulhalim, J. Opt. A, Pure Appl. Opt. **2**, L9 (2000).
[5] P. Yeh, *Optical Waves in Layered Media* (Wiley, New York, 1988).
[6] K. Tamasaku and T. Ishika, Acta Crystallogr., Sect. A: Found. Crystallogr. **A58**, 408 (2002).
[7] D. Felbacq, A. Moreau, and R. Smaali, Opt. Lett. **28**, 1633 (2003).
[8] S. Enoch, G. Tayeb, and D. Maystre, Opt. Commun. **161**, 171 (1999).
[9] E. R. Brown and O. B. McMahon, Appl. Phys. Lett. **67**, 2138 (1995).
[10] S. Fan, P. R. Villeneuve, and J. D. Joannopoulos, Phys. Rev. B **54**, 11 245 (1996).
[11] A. Serpenguzel, IEEE Microw. Wirel. Compon. Lett. **12**, 134 (2002).
[12] M. Golosovsky, Y. Neve-Oz, and D. Davidov, Synth. Met. **139**, 705 (2003).
[13] Y. Neve-Oz, M. Golosovsky, D. Davidov, and A. Frenkel, J. Appl. Phys. **95**, 5989 (2004).
[14] F. Abeles and P. Baumeister, Opt. Commun. **93**, 1 (1992).
[15] F. Abeles, J. Phys. Radium **19**, 327 (1958).
[16] A. V. Tikhonravov, P. W. Baumeister, and K. V. Popov, Appl. Opt. **36**, 4382 (1997).
[17] D. I. Babic and S. W. Corzine, IEEE J. Quantum Electron. **28**, 514 (1992).
[18] L. R. Brovelli and U. Keller, Opt. Commun. **116**, 343 (1995).
[19] E. Garmire, Appl. Opt. **42**, 5442 (2003).
[20] S. O'Brien and J. B. Pendry, J. Phys.: Condens. Matter **14**, 4035 (2002).
[21] H. F. Contopanagos, C. A. Kyriazidou, W. M. Merrill, and N. G. Alexopoulos, J. Opt. Soc. Am. A **16**, 1682 (1999).
[22] J. B. Pendry, Adv. Phys. **43**, 461 (1994).
[23] J. B. Pendry, A. J. Holden, W. J. Stewart, and I. Youngs, Phys. Rev. Lett. **76**, 4773 (1996).
[24] R. A. Shelby, D. R. Smith, S. C. Nemat-Nasser, and S. Schultz, Appl. Phys. Lett. **78**, 489 (2001).
[25] A. L. Pokrovsky and A. L. Efros, Phys. Rev. Lett. **89**, 093901 (2002).
[26] C. S. Kee, J. E. Kim, H. Y. Park, S. J. Kim, H. C. Song, Y. S. Kwon, N. H. Myung, S. Y. Shin, and H. Lim, Phys. Rev. E **59**, 4695 (1999).
[27] M. L. Povinelli, S. G. Johnson, J. D. Joannopoulos, and J. B. Pendry, Appl. Phys. Lett. **82**, 1069 (2003).
[28] J. Lam, J. Appl. Phys. **60**, 4230 (1986).
[29] A. K. Sarychev and V. M. Shalaev, Phys. Rep. **335**, 275 (2000).
[30] W. M. Merrill, R. E. Diaz, M. M. LoRe, M. C. Squires, and N. G. Alexopoulos, IEEE Trans. Antennas Propag. **47**, 142 (1999).
[31] B. Gralak, M. de Dood, G. Tayeb, S. Enoch, and D. Maystre, Phys. Rev. E **67**, 066601 (2003).
[32] M. Born and E. Wolf, *Principles of Optics*, 7th ed. (Cambridge University Press, Cambridge, 2002), p. 787.
[33] It is instructive to compare the values of n_A, Y_A found from the modeling of the reflectivity in terms of the Bragg reflector model, to predictions of, say, effective-medium theory. For the artificial dielectric consisting of a cubic array of perfectly conducting spheres embedded in the insulating matrix with $\epsilon_{\text{host}}, \mu_{\text{host}}$, the effective medium model (Ref. 29) predicts $\epsilon_{\text{eff}} = \epsilon_{\text{host}}(1+2p)/(1-p)$, $\mu_{\text{eff}} = \mu_{\text{host}}(2-2p)/(2+p)$ where p is the filling factor. In our case $p=0.28$. Assuming $\epsilon_{\text{host}}=1, \mu_{\text{host}}=1$, we find $\epsilon_{\text{eff}}=2.16$, $\mu_{\text{eff}}=0.63$. This should be compared to the experimentally found values of $\epsilon_A = n_A Y_A = 2.85$, $\mu_A = n_A/Y_A = 0.58$.
[34] ANSOFT Corp., Four Station Square, Suite 200, Pittsburgh, PA 15219, USA.
[35] CST GmbH, Budinger Str. 2a, 64289 Darmstadt, Germany.
[36] V. Yannopapas, A. Modinos, and N. Stefanou, Phys. Rev. B **60**, 5359 (1999).
[37] A. A. Krokhin, P. Halevi, and J. Arriaga, Phys. Rev. B **65**, 115208 (2002).
[38] P. Lalanne, Appl. Opt. **3**, 5369 (1996); Phys. Rev. B **58**, 9801 (1998).
[39] S. A. Tretyakov and A. J. Viitanen, J. Opt. Soc. Am. A **17**, 1791 (2000).
[40] S. M. Rytov, Yu. A. Kravtsov, and V. I. Tatarskii, *Principles*

of Statistical Radiophysics (Springer-Verlag, Berlin, 1987), Vol. 2, Chap. 4.

[41] K. M. Ho, C. T. Chan, and C. M. Soukoulis, Phys. Rev. Lett. **65**, 3152 (1990).

[42] E. Yablonovitch, T. J. Gmitter, and K. M. Leung, Phys. Rev. Lett. **67**, 2295 (1991).

[43] M. P. Silverman and R. B. Sohn, Am. J. Phys. **54**, 69 (1986).

[44] Z. Zhai, C. Kusko, N. Hakim, S. Sridhar, A. Revcolevschi, and A. Vietkine, Rev. Sci. Instrum. **71**, 3151 (2000).

[45] P. Sheng, *Scattering and Localization of Classical Waves in Random Media* (World Scientific, Singapore, 1990).